



JGR Earth Surface

,

RESEARCH ARTICLE

10.1029/2025JF008406

Key Points:

- We calculate endmembers from varietal data from zircons from sedimentary cover surrounding Cu-porphyry using Tucker-1 decomposition
- Endmembers indicate Cu-immobile (Source 1) or Cu-mobilizing (Source 2) sources; Source 2 proportions decrease with distance from orebodies
- Mathematical entities correspond to geological processes or entities indicating geological veracity of the Tucker-1 decomposition results

Supporting Information:

Supporting Information may be found in the online version of this article.

Correspondence to:

J. E. Saylor, jsaylor@eoas.ubc.ca

Citation:

Saylor, J. E., Richardson, N., Graham, N., Lee, R. G., & Friedlander, M. P. (2025). Tracking Cu-fertile sediment sources via multivariate petrochronological mixture modeling of detrital zircons. *Journal of Geophysical Research: Earth Surface*, 130, e2025JF008406. https://doi.org/10. 1029/2025JF008406

Received 14 MAR 2025 Accepted 11 SEP 2025

Tracking Cu-Fertile Sediment Sources via Multivariate Petrochronological Mixture Modeling of Detrital Zircons

Joel E. Saylor¹, Nicholas Richardson², Naomi Graham³, Robert G. Lee^{4,5}, and Michael P. Friedlander^{2,3}

¹Department of Earth, Ocean and Atmospheric Sciences, University of British Columbia, Vancouver, BC, Canada, ²Department of Mathematics, University of British Columbia, Vancouver, BC, Canada, ³Department of Computer Science, University of British Columbia, Vancouver, BC, Canada, ⁴Mineral Deposit Research Unit, University of British Columbia, Vancouver, BC, Canada, ⁵Now at BHP Ltd., Tucson, AZ, USA

Abstract Whereas the ability to acquire petrochronological data from detrital minerals has exploded, development of tools to analyze and interpret the multivariate data sets has not kept pace. Herein, we present a case study, which applies the recently developed non-negative Tucker-1 decomposition (NNT1) method to a multivariate detrital zircon data set from till samples collected above the Cu-bearing Guichon Creek Batholith in southern British Columbia, Canada. Zircon composition variables that we consider include age, Ce anomaly, Ce_N/Nd_N, Dy_N/Yb_N, ΔFMQ, Eu anomaly, ΣHREE/ΣMREE, Hf, Th/U, Ti temperature, and Yb_N/Gd_N. The NNT1 approach successfully deconvolves the multivariate data set into two endmembers, which are consistent with derivation either from non-oxidized and relatively anhydrous (i.e., low Cu-ore potential, Source 1) or oxidized and hydrous (i.e., potential Cu-ore bodies, Source 2) igneous rocks. Furthermore, we attribute each of the zircon grains to either the Source 1 or 2 endmember based on maximization of the likelihood that their measured multivariate geochemistry was drawn from one or the other of the learned multivariate endmembers. Finally, we demonstrate that the proportions of the Source 2 endmember decrease with increasing distance from the ore bodies, as expected due to down-ice or off-axis zircon mixing and dilution. We conclude that the NNT1 approach provides insight into geologically meaningful sediment transport processes and multivariate sediment sources even when those sources are unknown. It thus provides a basis for future petrochronological interpretations with applied and pure geoscience applications.

Plain Language Summary Few multivariate mathematical approaches exist to analyze the wealth of multivariate sediment provenance data being produced. Moreover, the results of mathematical models need to be correlated to geological reality before drawing geological conclusions. In this contribution, we test a recently developed multivariate "non-negative Tucker-1 decomposition" (NNT1) method by analyzing zircons from glacial sediments surrounding a known ore body. In this setting, we hypothesize that zircons should have geochemical characteristics either of the ore bodies or the non-ore bearing host rocks and that the abundance of zircons from the ore bodies should decrease with distance from the ore bodies. The results of data analysis using the NNT1 method support this hypothesis. Specifically, the NNT1 method suggests that there are two clearly distinguishable sources. The mathematical models of those sources' geochemical characteristics are consistent with derivation from either mineralized or non-mineralized igneous rocks. Furthermore, the modeled proportions of the modeled ore-body source decrease with increasing sample distance from the ore bodies. We conclude that the NNT1 method and the mathematical models which it produces correspond to geologically meaningful lithologies (i.e., real sediment sources) and geologically significant processes (i.e., down-ice sediment mixture and dilution).

1. Introduction

Petrochronology seeks to link chronology with specific rock-forming processes or conditions (Kohn et al., 2017). It is by its nature multidisciplinary and deals with multivariate data sets. Multiple approaches to petrochronology have been proposed, including many that focus on zircon and its trace and rare earth element (TREE) concentrations (Schaltegger and Davies, 2017). Multiple trace elements have been used to identify petrogenetic characteristics of source magmas, including crystallization temperature from Ti (Watson et al., 2006), metamorphic or igneous conditions (Hoskin & Schaltegger, 2003; Rubatto, 2002), crustal thickness from Eu anomaly or Sr/Y (Chapman et al., 2015; Sundell et al., 2022; Tang et al., 2020), or parent rock type from a suite of 26 trace elements

© 2025 The Author(s).

This is an open access article under the terms of the Creative Commons

Attribution-NonCommercial License, which permits use, distribution and reproduction in any medium, provided the original work is properly cited and is not used for commercial purposes.

SAYLOR ET AL. 1 of 16

(Belousova et al., 2002; Sundell et al., 2022). Trace element analysis of zircon also yields petrogenetic information about zircon source magmas and may therefore be useful for tracking crustal evolution or identifying orebearing lithologies (Dilles et al., 2015; Lee et al., 2017, Lee, Byrne, et al., 2021; Lu et al., 2016).

The multiple geochemical systems in zircon can also be exploited to identify and characterize sediment sources (Campbell et al., 2020; Smith, Saylor, Lapen, Hatfield, & Sundell, 2023). For example, due to the low diffusion of trace elements, U, Hf, and Th in zircon (Cherniak et al., 1997a, Cherniak et al., 1997b), as well as zircon's physical and chemical resilience, trace elements can be used as independent fingerprints of sediment provenance. Moreover, multiple studies have recognized that non-unique detrital zircon U-Pb age spectra present a challenge to identifying sediment sources or source proportions (Dickinson et al., 2009; Sundell et al., 2019). Some studies have introduced secondary parameters, including thermochronology, secondary isotopic analyses, or TREE analysis, to discriminate between otherwise similar sources (Campbell et al., 2005; Gehrels & Pecha, 2014; Saylor and Sundell, 2021; Smith, Saylor, Lapen, Hatfield, & Sundell, 2023).

However, the ability to acquire these multivariate data sets has outstripped development of tools to fully exploit and quantitatively compare or model multivariate zircon geochronology/geochemistry data sets. For example, forward (Monte Carlo) mixture modeling and bivariate non-negative matrix factorization methods have only recently been developed (Saylor and Sundell, 2021; Sundell and Saylor, 2017). While useful for conducting mixture modeling experiments or determining likely source area distributions of uni- or bivariate data sets, these applications cannot parse the complex interrelationships among TREE in order to fully exploit the multivariate nature of these data sets for sediment provenance, crustal evolution, or economic geology applications. Other multivariate approaches such as 3-way multidimensional scaling (MDS) or Generalized Procrustes Analysis (GPA) compare the relative similarity between empirical multivariate data sets but do not identify potential sediment source characteristics or mixing proportions (Vermeesch et al., 2023; Vermeesch and Garzanti, 2015). As part of their statistical validation of a recently developed non-negative Tucker-1 tensor decomposition (NNT1) method, Graham et al. (2025) successfully recovered known endmember distributions and proportions of a numerically generated varietal data set. However, the correlation between the calculated distributions or proportions and geological entities or processes has not been explored as it has been for other numerical methods such as forward mixing models or non-negative matrix factorization (e.g., Capaldi et al., 2017; Jackson & Horton, 2025; Saylor et al., 2013, 2019).

In this contribution, we use the recently developed, truly multivariate NNT1 method to analyze a suite of zircons from till samples within 15 km of ore-forming intrusions and porphyry Cu deposits in the Guichon Creek Batholith (GCB) in British Columbia (Figure 1) to test whether the method provides geologically meaningful endmember characterization and proportions. Our purpose is to test the suitability of the NNT1 method to determine sediment provenance and characterize mixing in sedimentary systems. Therefore, we limit our discussion of the NNT1 method to a conceptual overview and discussion of potential limitations (see Methods section below). For a full articulation and sensitivity testing of the NNT1 method, we refer readers to the original work by Graham et al. (2025).

We demonstrate that zircons from mixed samples (i.e., till) can be separated into endmembers which either include or exclude multiple geochemical features associated with porphyry Cu mineralization. We also demonstrate that the proportion of zircons derived from ore bodies decreases with distance down-ice or off-axis from the Cu deposits. Finally, we successfully invert the geochemical features to identify which grains are derived from the two groups. All of these point to the success of this tool at characterizing the rock-forming processes and conditions, even from detritus that has been eroded from its original location. It also points to the potential to use this tool for Cu porphyry exploration, particularly of Cu porphyry deposits which have been covered by subsequent alluvium.

2. Geological Setting

The GCB is a Late Triassic intrusion that consists of at least five concentrically zoned mafic-felsic intrusive phases. It intruded over \sim 11 Myr (218–207 Ma, D'Angelo et al., 2017; Lee, Byrne, et al., 2021) into Late Triassic basaltic to andesitic volcanic and volcaniclastic rocks of the Nicola Group, an island-arc assemblage that makes up the southern part of the Quesnel Terrane. Deposition of the Nicola Group (238–202 Ma) both precedes and post-dates intrusion of the GCB. The intrusive rocks become younger and more evolved from the margins to the core. The first intrusion in the region is the 217 Ma Gump Lake stock, and rocks in the core of the batholith are as

SAYLOR ET AL. 2 of 16

21699011, 2025, 10, Downloaded from https://agupubs.onlinelibrary.wiley.com/doi/10.1029/2025JF008406, Wiley Online Library on [09/11/2025]. See the Terms and Conditions (https://onlinelibrary.wiley.com/doi/10.1029/2025JF008406, Wiley Online Library on [09/11/2025]. See the Terms and Conditions (https://onlinelibrary.wiley.com/doi/10.1029/2025JF008406, Wiley Online Library on [09/11/2025]. See the Terms and Conditions (https://onlinelibrary.wiley.com/doi/10.1029/2025JF008406, Wiley Online Library on [09/11/2025]. See the Terms and Conditions (https://onlinelibrary.wiley.com/doi/10.1029/2025JF008406, Wiley Online Library on [09/11/2025]. See the Terms and Conditions (https://onlinelibrary.wiley.com/doi/10.1029/2025JF008406, Wiley Online Library.wiley.com/doi/10.1029/2025JF008406, Wil

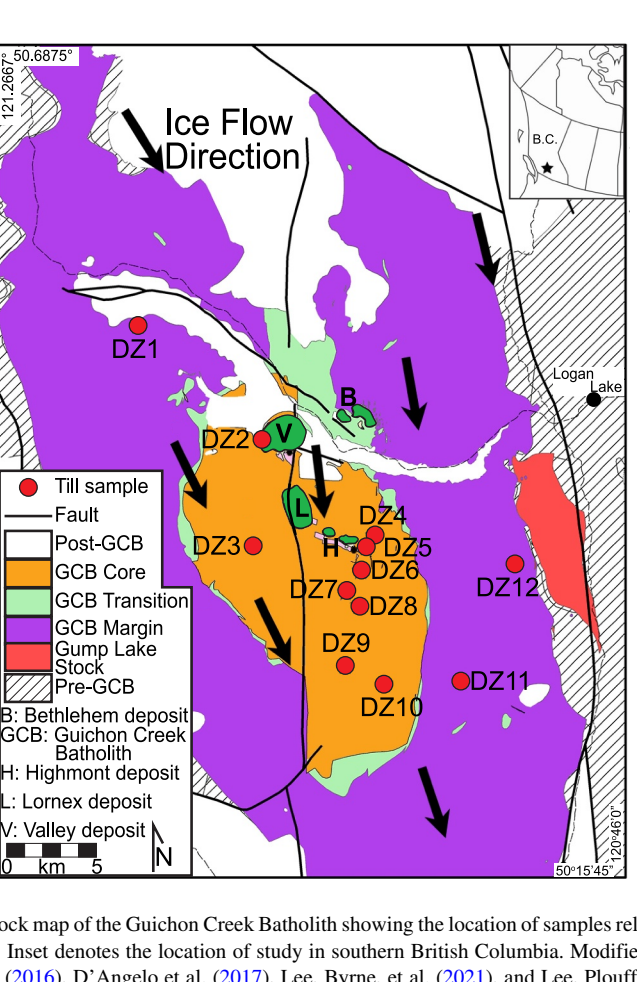


Figure 1. Simplified bedrock map of the Guichon Creek Batholith showing the location of samples relative to the ore deposits and the ice flow direction. Inset denotes the location of study in southern British Columbia. Modified after McMillan et al. (2009), Ferbey et al. (2016), D'Angelo et al. (2017), Lee, Byrne, et al. (2021), and Lee, Plouffe, et al. (2021).

young as 207 Ma (D'Angelo et al., 2017; Lee, Byrne, et al., 2021). There are multiple Cu-Mo mineralization centers in the core (Figure 1). Mineralization in the main centers is dated at 208.4 ± 0.9 Ma (Re-Os, D'Angelo et al., 2017).

The Guichon Creek region was covered by the Cordilleran ice sheet during the most recent glaciation between 28 and 11.5 ka. The Cordilleran ice sheet was formed by coalescence of alpine glaciers, which originated in regions such as the Coast and Canadian Rocky mountains (Clague & Ward, 2011). During the Last Glacial (Wisconsinan) Maximum (LGM), coalesced ice sheets flowing radially from ice domes in central British Colombia extended southward to just south of the 49th parallel (Arnold et al., 2016; Arnold & Ferbey, 2020; Clague & Ward, 2011; Ferbey & Arnold, 2013). Topography in the GCB region is characterized by rolling hills of the Interior Plateau (e.g., Ferbey et al., 2016). During the LGM, the region was occupied by an ice sheet, rather than by alpine glaciers, and so, ice flow was not controlled by local topography but rather by the location of the ice dome to the northwest of the study location. As a result, the ice flow direction was south-southwest (Figure 1). The direction of regional ice flow is based on the orientation of streamlined landforms (flutings, drumlins, crag-and-tails) and striations (Ferbey et al., 2016). Glaciation covered the region with <4-10 m of sub-glacial till, which was targeted for detrital zircon sampling (Lee, Plouffe et al., 2021; Plouffe et al., 2016).

Previous research using detrital mineral or chemical indicators of Cu mineralization focused on epidote and chalcopyrite abundances, Cu concentration, and zircon geochemical indicators. In this region, Casselman et al. (1995) found that epidote is present in a 20-km wide regional halo around the mineralized zones. Beyond that regional trend, there appears to be no correlation between the concentration of epidote and distance to the mineralized zones (Plouffe et al., 2016). Chalcopyrite abundance and Cu concentration show inconsistent trends. There is an increase in both chalcopyrite abundance and Cu concentration approaching the mineralized zones, but there are counterexamples where there is an increase in both chalcopyrite and Cu concentration away from the

SAYLOR ET AL. 3 of 16

21699011, 2025, 10, Downloaded from https://agupubs.onlinelibrary.wiley.com/doi/10.1029/2025JF008406,

Journal of Geophysical Research: Earth Surface

mineralization zones (Plouffe et al., 2016). Hence, in the case of chalcopyrite and Cu concentration, there appear to be as many false as true positives. Lee, Plouffe et al. (2021) qualitatively characterized a decrease in Eu anomaly in detrital zircon samples down-ice of the ore bodies in the GCB, providing the motivation for further quantifying the relationship.

3. Methods

3.1. Zircon Petrochronology

Twelve till samples were collected within the GCB at distances of 0.25-15 km down-ice from mineralization (Figure 1, Ferbey et al., 2016). Samples were collected at depths of 130-150 cm below the surface from wellcompacted, massive, and generally fissile cobble-boulder diamictic conglomerates with abundant striated clasts in a clay-rich, silty-sand to sandy-silt matrix (Figure 1; Ferbey et al., 2016). These deposits are interpreted as a subglacial till facies. Following methods described by Plouffe et al. (2013), sampling targeted the matrix and excluded clasts larger than fine pebbles. Zircons were separated from 9 to 15 kg till samples using standard density and magnetic methods (Ferbey et al., 2016). Between 14 and 31 zircon grains per sample were mounted in epoxy and analyzed by laser ablation-inductively coupled plasma mass spectrometry at the Pacific Centre for Isotopic and Geochemical Research at the University of British Columbia (Lee, Plouffe et al., 2021). Although lower than standard sample size for detrital zircon samples, analysis was limited by the availability of zircons from the samples. We address the potential impacts and caveats arising from the small sample size in the Discussion section. At least two spots were analyzed per grain and geochemical concentrations and ratios were calculated using the methodology described in Lee, Plouffe et al. (2021), resulting in 20–60 analyses per sample. We calculated the distance from the edge of the nearest ore body in both the down ice-flow direction and also the off-axis direction orthogonal to the ice-flow direction. Following analysis using the NNT1 algorithm, we compare variables to those in either mineralized or non-mineralized igneous bedrock using data reported by D'Angelo et al. (2017) and Lee, Byrne, et al. (2021).

3.2. Geochemical Indicators of Copper-Fertile Magmas

Cu mineralization is associated with evolved, oxidized, and hydrous magmas, often those which originate in thick crust (Lee & Tang, 2020). We therefore use multiple geochemical systems to track these features and assess the potential of endmember sources to mobilize Cu and precipitate Cu-bearing minerals. In oxidized magmas that form porphyry Cu deposits, zircons are characterized by Eu anomalies (Eu/Eu_N*) > \sim 0.3–0.4 (Dilles et al., 2015; Lee, Byrne, et al., 2021, Lee, Plouffe et al., 2021; Lu et al., 2016). This relationship is complicated by recent research that suggests that zircon Eu/Eu_N* is also correlated to thicker crust (Tang et al., 2020) because thick crust suppresses plagioclase crystallization and can yield the same signal. That Cu fertile zones in the GCB are associated with high Yb_N/Gd_N (>15) (Bouzari et al., 2020) contrasts with observations that Cu-bearing igneous rocks are typically depleted in heavy REE (HREE) due to early growth of garnet in the magma chamber under thick crust (Bissig et al., 2017; Loucks, 2014). The apparent disconnect between HREE/MREE ratios and Cu mineralization may provide a method of discriminating Cu mineralization in thin versus thick crust. Highly oxidized magmas should yield more Ce in its Ce⁴⁺ oxidized state which is compatible in zircon. Zircon from these magmas should therefore have high Ce concentrations and therefore high Ce_N/Nd_N and Ce anomalies (Ballard et al., 2002; Lu et al., 2016) as well as high ΔFMQ values (Loucks et al., 2020). However, follow-up research has questioned the efficacy of Ce anomaly and Ce_N/Nd_N for tracking Cu mineralization (Loader et al., 2022) and highlighted overlap in ΔFMQ between mineralized and non-mineralized plutons (Loucks et al., 2024).

Cu tends to precipitate from evolved magmas during late-stage magmatism, and so, Cu-fertile porphyries tend to be associated with lower temperature magmas. We track magma temperature using the Ti-in-zircon geothermometer of Watson et al. (2006) with an α_{TiO2} of 0.7 to allow for rutile understaturation. We track magma evolution using zircon Th/U and [Hf], which are expected to decrease and increase, respectively, during early fractional crystallization of apatite, hornblende and titanite. Thus, Cu fertile zones in the GCB tend to be associated with low Th/U (<0.45) and high but not extreme [Hf] (8,750 < Hf < 11,720 ppm, Pizarro et al., 2020; Carrasco-Godoy et al., 2024).

Finally, Cu mobilization requires hydrous magmas, which also favor early crystallization of hornblende. Hornblende crystallizes at an early stage in hydrous melts and preferentially scavenges Y and middle rare earth

SAYLOR ET AL. 4 of 16

elements, resulting in high Hf/Y and low Dy_N/Yb_N in most ore bodies (Davidson et al., 2007; Lee, Byrne, et al., 2021; Lu et al., 2016; Moore and Carmichael, 1998; Sisson, 1994).

In summary, a suite of 11 variables, including U-Pb age, Ce anomaly, Ce_N/Nd_N , Dy_N/Yb_N , ΔFMQ , Eu anomaly, $\Sigma HREE/\Sigma MREE$, Hf, Th/U, Ti temperature, and Yb_N/Gd_N from 12 detrital zircon samples from locations surrounding the GCB (Figure 1, Table S1) were used to determine whether there is a consistent discrimination between zircons from potentially Cu-mobilizing versus Cu-immobile sources.

3.3. Tucker-1 Decomposition

We determine the most likely number of sedimentary sources (a.k.a., the optimum rank) as well as the distribution of each of the 11 variables in each source using the NNT1 method (Graham et al., 2025). The method yields three key insights into the data, the second and third of which cannot be obtained by any other method currently available. First, it indicates the most likely number of sources from which the mixed samples were drawn by calculating the optimum rank. Second, it yields the distribution of each of the variables in each source. Third, it calculates the proportion of each source present in each mixed sample using two methods. All calculations were conducted in DZgrainalyzer (http://dzgrainalyzer.eoas.ubc.ca/), a free web-based application built on the code described by Graham et al. (2025).

We describe the unsupervised NNT1 method below with reference to our data set of 11 variables from 12 detrital samples using the steps below. First, the 11 variables were converted to kernel density estimates (KDEs) following the methods outlined by Graham et al. (2025) (Figure 2a, Table S2). Construction of KDEs follows standard procedures, whereby an optimum bandwidth was selected and uniformly applied for each variable from all samples. Hence, for example, all [Hf] data are treated with a uniform bandwidth, but a different bandwidth is used for all age data. Data points were converted to Gaussian curves using the data point as the mean and the bandwidth as the standard deviation. Gaussian curves for each sample were normalized by summing individual Gaussian curves and dividing the summed curve by the number of observations for that sample. Next, KDEs were discretized over K points and compiled into a 3-way tensor of empirical data, Y of size $I \times J \times K$, where I is the number of sink samples (in this Case 12) and J is the number of variables (a.k.a., features, in this Case 11) (Figure 3). Finally, the NNT1 algorithm approximates Y as

$$Y = A \times B + E, \tag{1}$$

where A is the proportions matrix (with size $I \times R$), B is the source tensor (with size $R \times J \times K$), R is the number of sources considered (a.k.a., rank), and E is the misfit between model tensor Y (that is, $A \times B$) and empirical tensor Y. The algorithm improves the fit between Y and Y by alternatively holding A or B constant while modifying the other via projected-gradient step to minimize E.

The method described above is both robust and versatile. Testing using multiple KDE bandwidths indicates that the selected rank, A_{ir} , and B_{rjk} are not affected by bandwidth selection, the number of variables, or the number of points over which the KDE is discretized (see figure 6 in Graham et al., 2025). Testing by Graham et al. (2025) indicates that there is a mean residual error of only 9% between known and estimated KDEs and a mean absolute error of only \sim 5% between known and estimated proportions. Conversion to KDEs maximizes the versatility of the method because it means that samples can be compared regardless of the number of analyses per sample and that any variable that can be represented as a distribution can be included in the data set (Graham et al., 2025).

In order to estimate the optimum rank, we repeated the NNT1 decomposition for ranks 1-12 (i.e., between 1 and 12 sources) and calculated the misfit (E) between model tensors (Y) and the empirical data (Y) for each rank. Conceptually, the optimum rank is that rank which accounts for the empirical data with the simplest model. Practically, the optimum rank is selected at the "knee" in the misfit-versus-rank graph, where there is a marked reduction in improvement in misfit with additional ranks. When evaluated using numerically generated samples, the algorithm identified the correct rank (i.e., the correct number of sources), even with as few as double the number sinks as sources (Graham et al., 2025). Given our sample size of 12, this suggests that the algorithm should be able to robustly discriminate the ideal rank for ranks between one and six.

We estimate the proportions of each endmember in the 12 detrital samples using two methods. The first method takes the proportions directly from the proportions matrix (A above). The second method uses the ratio of

SAYLOR ET AL. 5 of 16

21699011, 2025, 10, Downloaded from https://agupubs.onlinelibrary.wiley.com/doi/10.1029/2025JF008406, Wiley Online Library on [09/11/2025]. See the Terms and Conditions (https://onlinelibrary.wiley.com/terms-and-conditions) on Wiley Online Library for rules of use; OA arcicles are governed by the applicable Creative

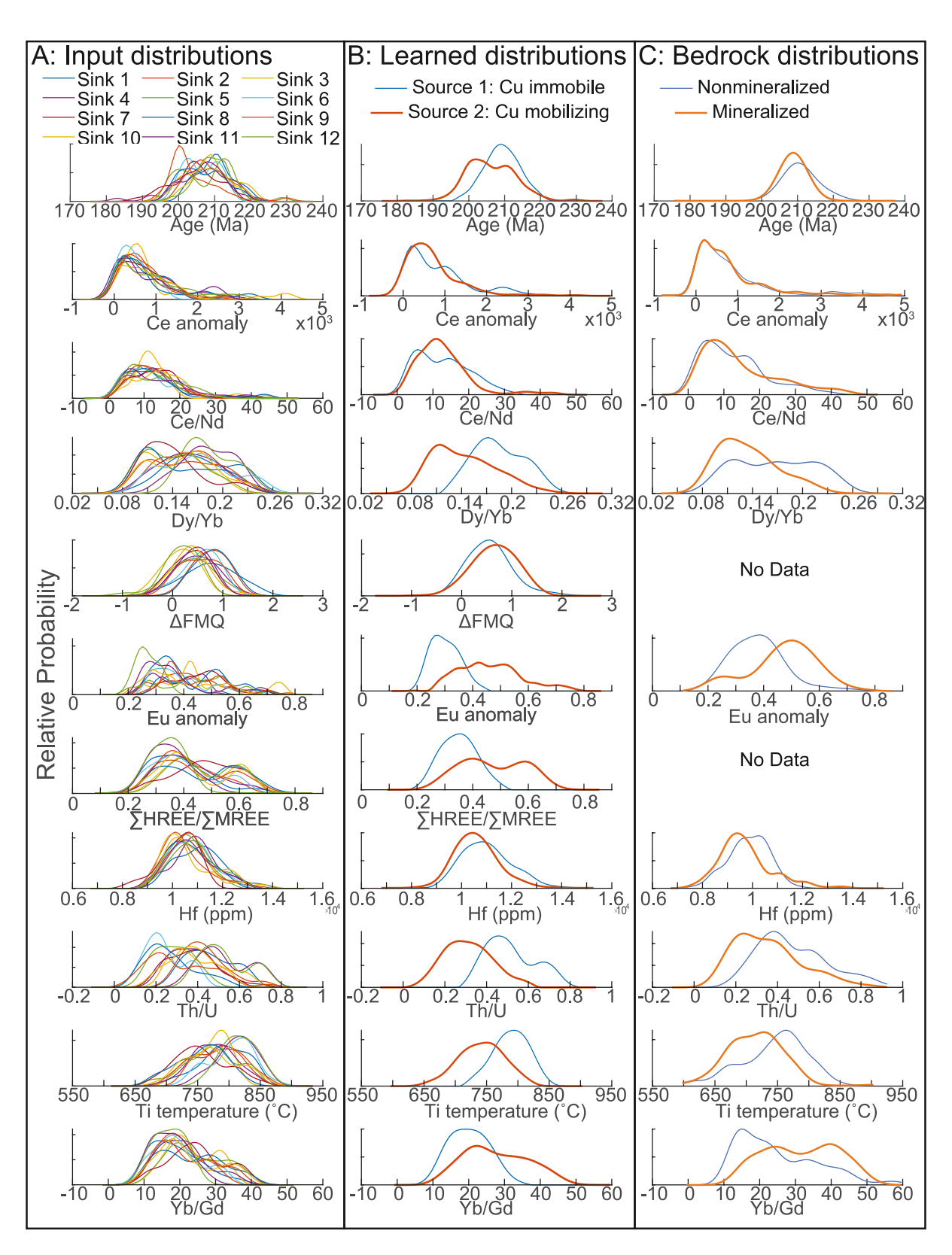


Figure 2. (a) Empirical distributions of 11 variables from 12 samples used as input to the non-negative Tucker-1 decomposition (NNT1) algorithm. (b) Endmember distributions for each of the 11 variables learned by the NNT1 algorithm. (c) Empirical distributions of variables in bedrock data from the Guichon Creek Batholith for comparison to learned endmembers. Data for C are from D'Angelo et al. (2017) and Lee, Byrne, et al. (2021). Data presented in this figure are available in Tables S2 and S4.

SAYLOR ET AL. 6 of 16

21699011, 2025, 10, Downloaded from https://agpubs.onlinelibrary.wiley.com/doi/10.10292025JF008406, Wiley Online Library on [09/11/2025]. See the Terms and Conditions (https://onlinelibrary.wiley.com/terms-and-conditions) on Wiley Online Library for nels of use; OA articles are governed by the applicable Creative Commons Licensen

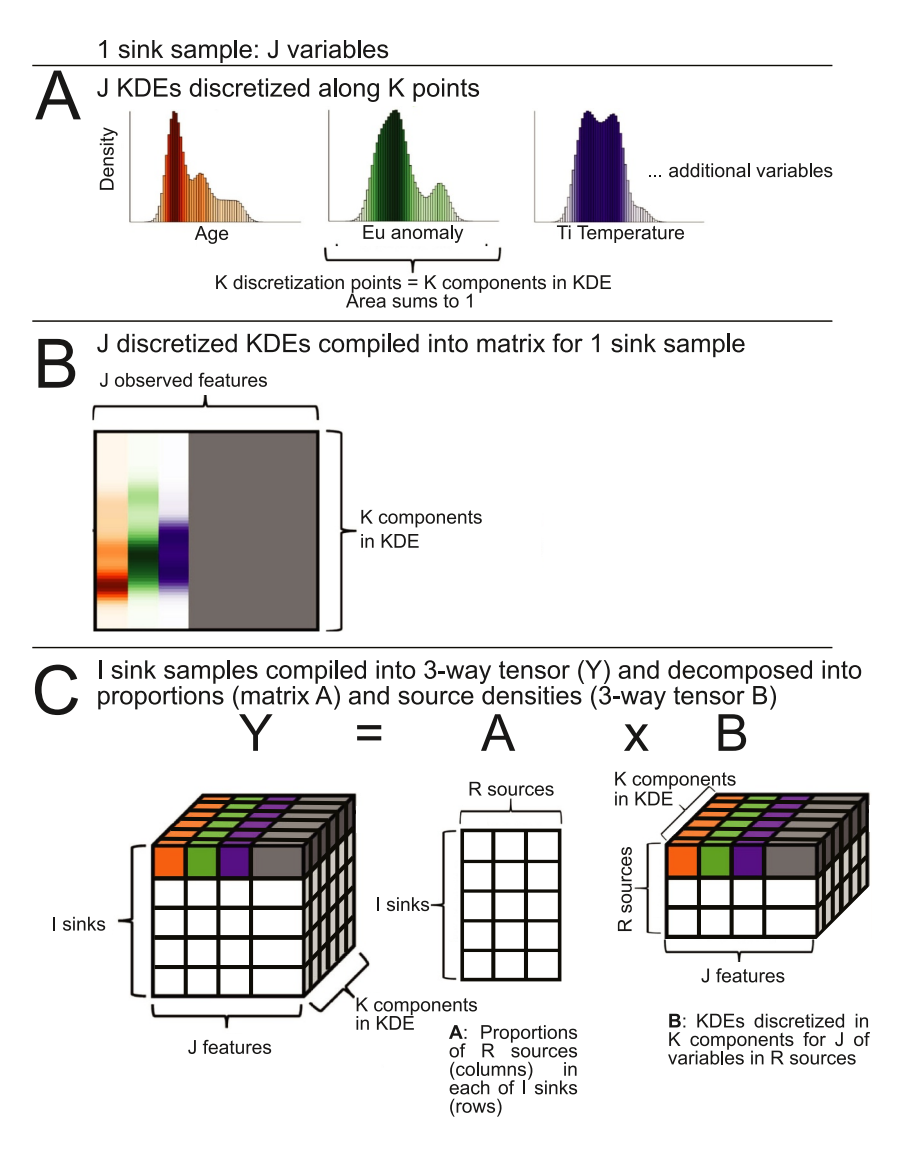


Figure 3. Conceptual presentation of (a) discretization of empirical kernel density estimates (KDEs) and (b) compilation into one matrix per sample. (c) Matrices from each sample are assembled into a 3-way tensor (Y), which is the basis for decomposition into a proportions matrix (a) and source KDE 3-way tensor (b). Modified from Graham et al. (2025).

likelihoods method (Graham et al., 2025) to determine the most likely source for each zircon grain analyzed by comparing that sample's 11 variables to the distributions of those variables estimated for each source. This approach calculates the likelihood that every variable in each grain was drawn from the distributions associated with either Source 1 or Source 2 and selects the maximum likelihood as the likely source. We compared these grain labels to the mixing proportions of individual sample's KDEs in matrix Air. We also compared the grain labeling to the results of an independent Classification and Regression Tree (CART) analysis designed to characterize zircon grains as coming from either a Cu "fertile" or Cu "barren" source based on their geochemistry (Carrasco-Godoy et al., 2024). For the CART analysis, we used a subset of five variables, including Eu anomaly, Th/U, Ce/Nd, Dy/Yb, and Gd/Yb, and applied the method using the online app developed by Carrasco-Godoy et al. (2024) and available at ccarr.shinyapps.io/Zircon_fertility_models/. For this combination of variables, Carrasco-Godoy et al. (2024) report a sensitivity, defined as the proportion of zircons indicating Cu fertility correctly attributed to the "fertile zircon" class, of ~70% and a specificity, defined as the proportion of zircons indicating Cu infertility correctly attributed to the "barren zircon" class, of ~90%. For comparison, testing by Graham et al. (2025) using numerical data sets with either two or seven variables yield grain-label accuracy of 76.1% and 88.5%. The trend of greater labeling accuracy with greater numbers of variables suggests that a data set with even more variables, such as ours, should yield even greater grain-label accuracy.

SAYLOR ET AL. 7 of 16

21699011, 2025, 10, Downloaded from https://agupubs.onlinelibrary.wiley.com/doi/10.1029/2025JF008406, Wiley Online Library on [09/11/2025]. See the Terms and Condition

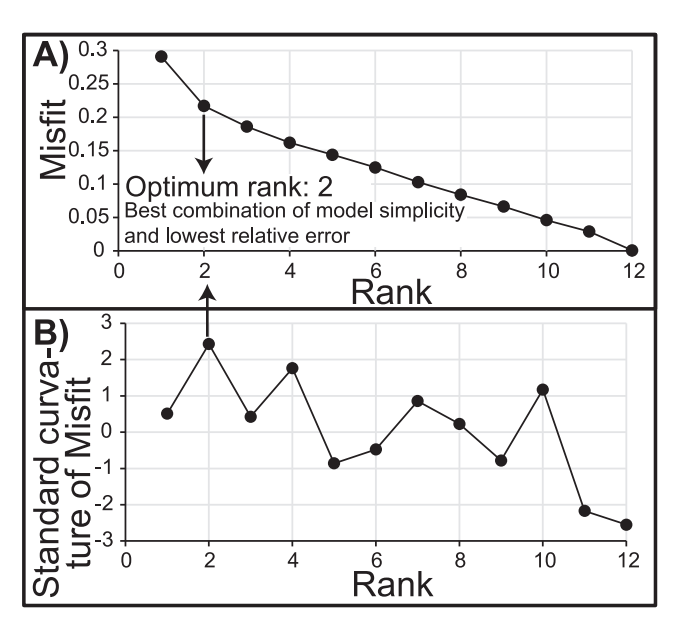


Figure 4. (a) Misfit between modeled tensor (a) \times (b) and the true tensor (Y), calculated as E in Equation 1 for ranks between 1 and 12. (b) Standard curvature of Misfit versus Rank curve. The optimum rank is identified as a "knee" in (a), which corresponds to a maximum in (b). Data presented in this figure are available in Table S3.

In order to highlight the difference between the NNT1 method used in this research and the primary alternative multivariate sediment provenance analysis approach, we applied 3-way Multidimensional Scaling (MDS, Carroll & Chang, 1970) and GPA (Gower, 1975) to this data set using the Provenance software package (Vermeesch et al., 2023; Vermeesch and Garzanti, 2015). These approaches break the data set into 11 distributional data sets, each with 12 samples. The KS-statistic is calculated to enable intercomparison of the 11 distributional data sets, and applies GPA to the resulting 3-way tensor of dissimilarity values.

4. Results

Converting the 11 variables for the 12 samples to KDEs yields the distributions in Figure 2a. Based on a decrease in the slope of the misfit with respect to rank, the algorithm identified rank 2 as the optimum rank, which accounts for the input variables while maintaining the simplest model (Figure 4a, Table S3). Decomposition of the data set into two sources (i.e., rank 2), yielded the distributions in Figure 2b, and the proportions in Figure 5 (Tables S4 and S5). For eight of the 11 variables, the endmember KDEs consistently discriminate between a source in which Cu is likely immobile (Source 1) and a potentially Cu-mobilizing source (Source 2) (Figure 2b, Table S4). For example, Source 2 is associated with low age, low $\mathrm{Dy_N/Yb_N}$, high Eu anomaly, high $\mathrm{\Sigma HREE/\Sigma MREE}$, intermediate Hf, low Th/U, low Ti temperature, and high Yb/Gd (Figure 2b). $\mathrm{\Delta FMQ}$ shows limited discrimination with the Cu-mobilizing Source 2 having only a slightly higher modal $\mathrm{\Delta FMQ}$. Although Ce anomaly and Ce/Nd do not discriminate between Cu-mobilizing and Cu-immobile sources, they are not inconsistent with the results from the other variables.

The proportions of Source 2 based on the NNT1 method are directly proportional (though slightly greater than) the proportions of Source 2 based on the grain labeling (Figure 6b, Tables S5 and S6). Nevertheless, both methods show the same down-ice stream decrease in the proportions of Source 2 (Figure 5, Table S5). Finally, there is \sim 80% overlap between the source attributions based on the CART analysis and the grain-source identification based on the NNT1 method (Figure 6c, Table S6).

The results of GPA are broadly similar to the distribution of the proportion of Source 2 identified by the NNT1 approach (Figure 7, Table S7). However, GPA does not identify the characteristics of the endmembers, and so, the GPA plot reveals less about the samples or their possible sources than the proportions of the Source 2 plot does.

3-way MDS produces two sets of coordinates: one set for the Group Configuration which situates the samples in Cartesian space and another set of coordinates for the Source Weights which is based on the degree to which

SAYLOR ET AL. 8 of 16

21699011, 2025, 10, Downloaded from https://agupubs.onlinelibrary.wiley.com/doi/10.1029/2025/F008406, Wiley Online Library on [09/11/2025]. See the Terms and Conditions (https://onlinelibrary.wiley.com/terms

and-conditions) on Wiley Online Library for rules of use; OA articles are governed by the applicable Creative

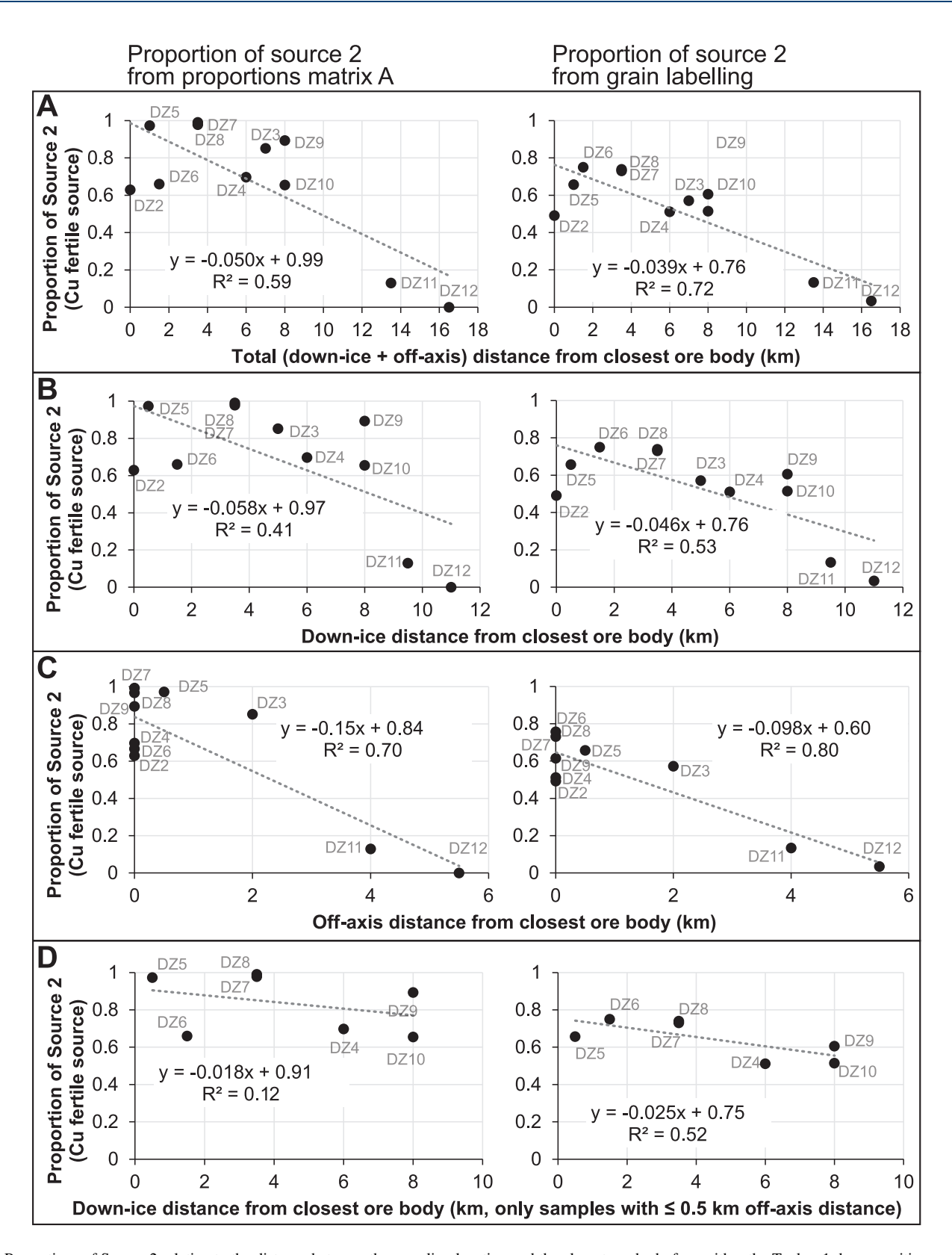


Figure 5. Proportions of Source 2 relative to the distance between the sampling location and the closest ore body from either the Tucker-1 decomposition method or based on attribution of each grain to either Source 1 or Source 2. Panel A shows the total distance calculated as down-ice + off-axis distance for all samples. Panel B shows only the down-ice distance for all samples. Panel C shows only the off-axis distance for all samples. Panel D shows the down-ice distance for samples with \le 0.5 km off-axis distance. Data presented in this figure are available in Table S5.

SAYLOR ET AL. 9 of 16

21699011, 2025, 10, Downloaded from https://agupubs.onlinelibrary.wiley.com/doi/10.1029/2025JF008496, Wiley Online Library on [09/11/2025]. See the Terms and Conditions (https://onlinelibrary.wiley.com/ems-and-conditions) on Wiley Online Library for rules of user; OA articles are governed by the applicable Creative Commons Licensea

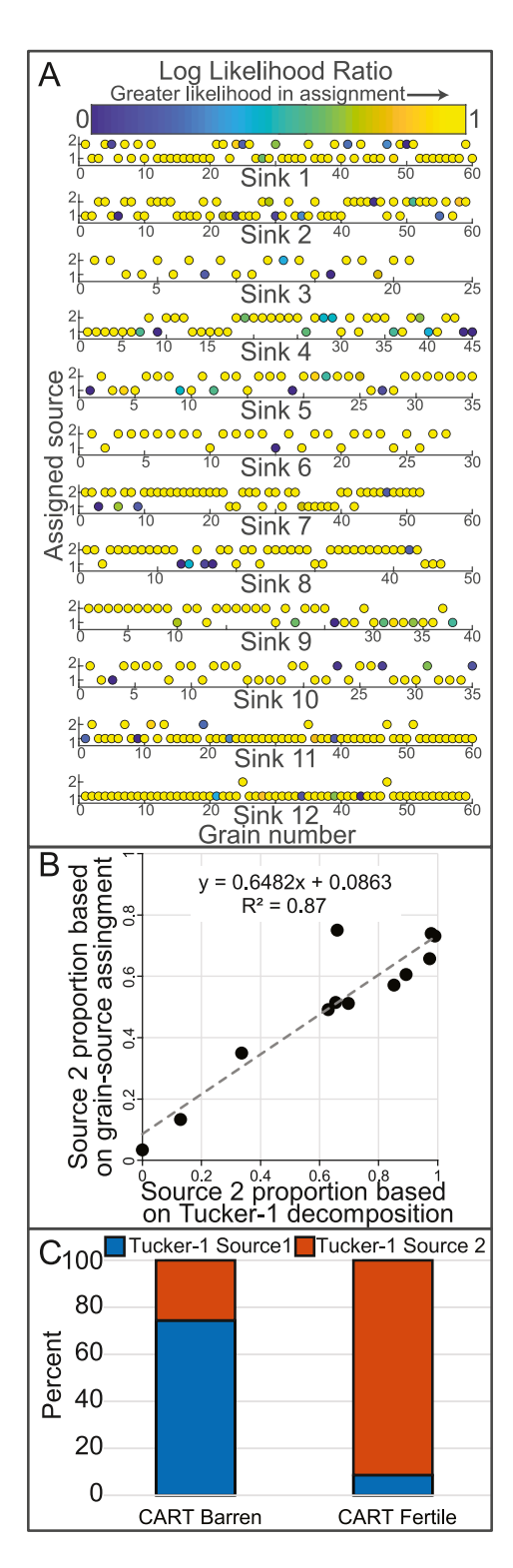


Figure 6. (a) Categorization of each input zircon grain based on maximization of the likelihood that the measured multivariate data originate from one of the learned multivariate source distributions (Figure 2B). Grains are colored by the log ratio between the most likely source and the second most likely source. A log ratio value of 1 indicates that it is 10 times more likely that the grain was drawn from the assigned source than the alternative and a value near 0 indicates that either source is roughly equally likely. (b) Source 2 proportions based on the tensor decomposition (matrix A_{ir} in Equation 1) or the grain-source assignment yield comparable results. (c) Comparison between grain-source assignment based on the Tucker-1 method to an ore-exploration specific Classification and Regression Tree analysis indicates \sim 80% overlap in source attribution. Data are available in Tables S5 and 6.

SAYLOR ET AL. 10 of 16

specific variables impact the group configuration. For example, variables Ce/Nd, Δ FMQ, and Ce anomaly are heavily weighted in the *Y* direction (Figure 8b), suggesting that they primarily control the samples' locations in the *Y* direction in the Group Configuration plot (Figure 8a). In contrast, variables Dy/Yb, Yb/Gd, and Δ HREE/ Δ MREE are heavily weighted in the *X* direction, suggesting that they have strong discriminatory power in the *X* direction in the Group Configuration panel.

5. Discussion

The results above confirm that endmember characteristics in tensor B_{rjk} are geologically meaningful. Eight of 11 of the endmember distributions are consistent with Source 2, representing derivation from hydrous, evolved, and oxidized magmas in which Cu might be mobile (Figure 2b). For the other three variables, the endmember KDEs broadly overlap, consistent with previous research suggesting that they are of limited value in discriminating Cumobilizing magma bodies (Figure 2b). Notably, the estimated KDEs closely match empirical KDEs of data from zircons from mineralized and non-mineralized bedrock reported by D'Angelo et al. (2017) and Lee, Byrne, et al. (2021) (c.f., Figures 2b and 2c). The KDEs for each of the seven variables that yield clear discrimination between Source 1 and Source 2 are matched by empirical observation from either mineralized or non-mineralized local bedrock (Figures 2b and 2c). On the other hand, the two variables whose endmember KDEs do not discriminate between are also matched by empirical observations that those variables do not reliably separate mineralized versus non-mineralized bedrock (c.f. Ce anomaly and Ce/Nd in Figures 2b and 2c).

The proportion of Source 2 is inversely proportional to down-ice and off-axis distance from the ore bodies, as expected if Source 2 is in fact related to GCB Cu-fertile ore bodies (Figure 5). The down-ice decrease in Source 2 is observed when considering only the down-ice distance (i.e., excluding the off-axis distance) for all samples (Figure 5b) and also when considering only those samples with an off-axis distance <0.5 km (Figure 5d). As expected, the decrease in proportions of Source 2 is also inversely proportional to the off-axis distance from the nearest ore body (Figure 5c). The decrease in Source 2 is consistent with down-ice or off-axis sediment dilution (Clark, 1987; Iverson et al., 1996; Schaetzl et al., 2020) as observed, for example, in the down-ice decrease in ¹⁰Be concentrations in Alaskan glaciers (Matmon et al., 2020). The off-axis spatial trend of the proportion of Source 2 is more pronounced than the down-ice trend, with gradients of -0.098 to -0.15 km⁻¹ versus -0.018 to -0.025 km⁻¹, respectively (c.f., Figures 5c and 5d). The off-axis trend also has a larger correlation with the proportion of Source 2 than the down-ice trend, with R² values of 0.7–0.8 versus 0.12–0.5, respectively (c.f., Figures 5c and 5d). These trends are consistent with sediment transport largely along, rather than orthogonal to, the ice-flow direction. Down-ice changes in the concentration of sediment sources are typically attributed to a combination of mechanical comminution and dilution by deposition of bed load and erosion of bedrock during down-ice transport (Clark, 1987). Because zircon grains are not subject to significant comminution, we attribute the decrease in the proportion of Source 2 to dilution via deposition and erosion. The consistency between the numerical results and empirical observations of down-ice mixing and dilution during glacial sediment transport confirms that the relative proportions in matrix A_{ir} are geologically meaningful. The proportions of Source 2 based on the NNT1 method are directly proportional (though slightly greater than) the proportions of Source 2 based on the grain identification (Figure 6b). Nevertheless, both methods show the same down-ice and off-axis decrease in the proportions of Source 2 (Figure 5).

In addition to yielding geologically reasonable results, the NNT1 method yields results that are consistent with independent, application-specific methods (Figure 6c). Specifically, there is close correlation between the grains attributed to Cu-immobile (Source 1) verses Cu-mobilizing (Source 2) compared to their attribution based on the ore exploration-specific CART application. The correlation is remarkable given the CART sensitivity of \sim 70% and specificity of \sim 90% and the 76%–89% accuracy of the grain-labeling method (Carrasco-Godoy et al., 2024; Graham et al., 2025). This relationship suggests that even though the NNT1 method is broadly applicable to varietal data treated "as columns" (Method 2 of Vermeesch et al., 2023) it's performance is comparable to application-specific methods.

These results are also broadly consistent with a 3-way MDS and GPA treatment of the data but provide additional insight into the geochemical composition of likely endmembers. Whereas 3-way MDS, GPA, and the NNT1 method broadly separate samples by the proportion of Source 2 present in the samples (compare Figures 7a, 8b, and 8a), the NNT1 method also provides insights into the potential sources of the mixed sink samples being investigated. The 3-way MDS analysis reveals more about the data set than the GPA, consistent with the

SAYLOR ET AL.

21699011, 2025, 10, Downloaded from https://agupubs.onlinelibrary.wiley.com/doi/10.1029/2025JF008406, Wiley Online Library on [09/11/2025]. See the Terms and Conditions (https://onlinelibrary.wiley.com/doi/10.1029/2025JF008406, Wiley Online Library on [09/11/2025]. See the Terms and Conditions (https://onlinelibrary.wiley.com/doi/10.1029/2025JF008406, Wiley Online Library on [09/11/2025]. See the Terms and Conditions (https://onlinelibrary.wiley.com/doi/10.1029/2025JF008406, Wiley Online Library on [09/11/2025]. See the Terms and Conditions (https://onlinelibrary.wiley.com/doi/10.1029/2025JF008406, Wiley Online Library on [09/11/2025]. See the Terms and Conditions (https://onlinelibrary.wiley.com/doi/10.1029/2025JF008406, Wiley Online Library on [09/11/2025]. See the Terms and Conditions (https://onlinelibrary.wiley.com/doi/10.1029/2025JF008406, Wiley Online Library on [09/11/2025]. See the Terms and Conditions (https://onlinelibrary.wiley.com/doi/10.1029/2025JF008406, Wiley Online Library.wiley.com/doi/10.1029/2025JF008406, Wiley Online Library.wiley.com/doi/1

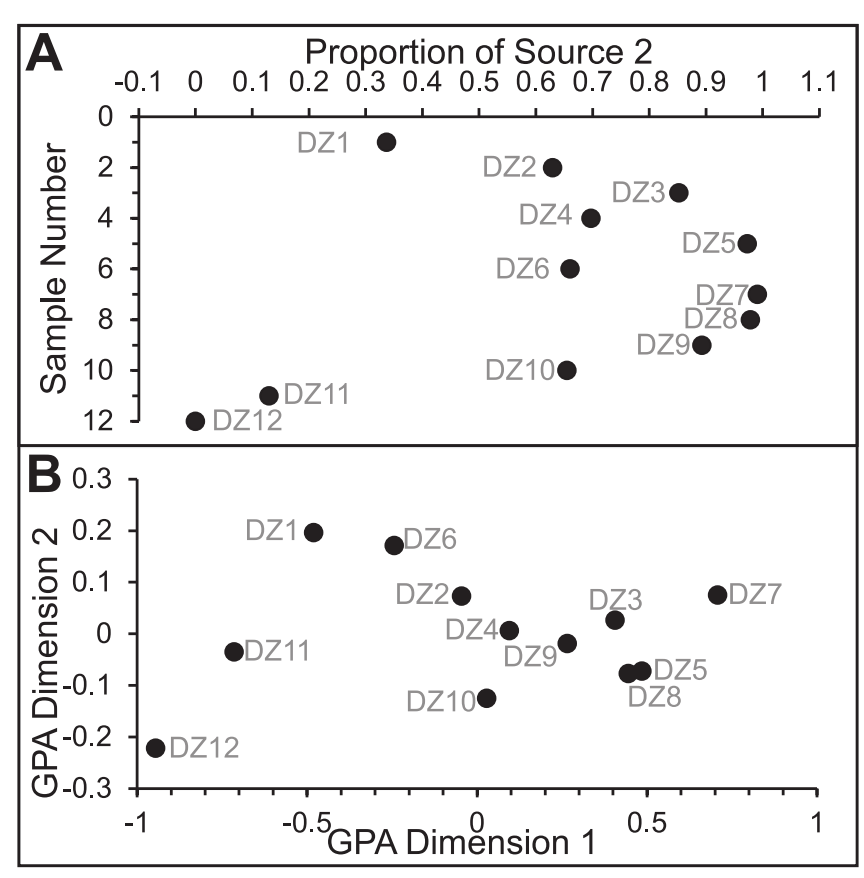


Figure 7. A similar distribution is obtained by comparison Generalized Procrustes Analysis (GPA) and the proportions of Source 2. (a) A plot of the proportions of Source 2 identified by Tucker-1 decomposition by sample number. (b) Generalize Procrustes Analysis applied to the data set of 11 variables for the 12 till detrital zircon samples. The data set was broken into 11 distributional data sets, each with 12 samples following Method 2 of Vermeesch et al. (2023) and subject to GPA following methods outlined by Vermeesch and Garzanti (2015). Data in this figure are available in Tables S5 and S7.

conclusions of Vermeesch et al. (2023). The Group Configuration (Figure 8a) indicates that the data set is more heavily discriminated along the X direction and therefore the Y direction has limited discriminatory power. This is consistent with the observed broad overlap in the distributions of variables that are heavily weighted in the Y direction in the Source Weights figure (Figure 8b), including Ce/Nd Ce/Ce* and Δ FMQ, between Source 1 and Source 2 identified by the NNT1 method (Figure 2b). On the other hand, the greater discrimination along the X direction is consistent with the broad separation between the distributions of Yb/Gd, Dy/Yb, Σ HREE/ Σ MREE in Source 1 and Source 2 as determined by the NNT1 method. However, despite the greater interpretive power of 3-way MDS over GPA, it still does not yield insight into the distribution of the variables in the potential sediment sources nor does it provide quantitative mixing proportions of those potential sources into the sink samples. Furthermore, it does not assign grains to individual sources as the maximum likelihood approach does (Figure 5a). Both GPA and 3-way MDS are useful for comparison of complex, empirical, multivariate, and detrital provenance data sets, but neither of them provides a basis for petrochronological characterization of potential sediment sources or quantitative mixture modeling of detrital compositions. They are therefore complementary but not directly comparable to the NNT1 method due to their different goals and methods.

Although the data set is limited to only 14–31 (median = 22) grains per sample, it benefits from the multivariate nature of the data set, from multiple analyses per grain, and from a constrained geological setting where the endmembers are clearly delineated. Inclusion of 11 variables per sample effectively enlarges the data set to 154–341 (median = 242) analyses per sample, which approaches the n = 300 recommendation for quantitative detrital zircon analysis (Saylor and Sundell, 2016). Inclusion of multiple analyses per grain yields confidence that the KDEs reflect the underlying distribution and minimizes the chance of any specific analysis skewing the KDE. Finally, the primary reason to use this data set despite its small size is that it comes from a well-characterized,

SAYLOR ET AL. 12 of 16

21699011, 2025, 10, Downloaded from https://agupubs.onlinelibrary.wiley.com/doi/10.1029/2025JF008406, Wiley Online Library on [09/11/2025]. See the Terms and Conditions (https://onlinelibrary.wiley.com/term

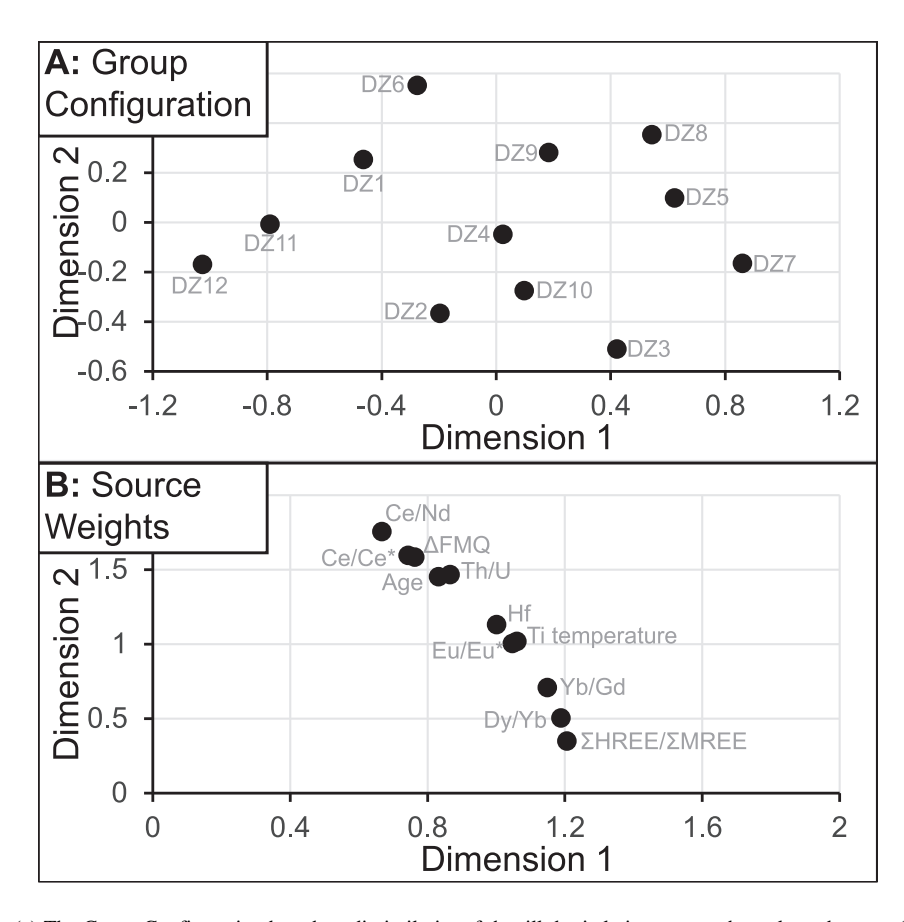


Figure 8. (a) The Group Configuration based on dissimilarity of the till detrital zircon petrochronology data set. (b) The Source Weights of the variables in the till detrital zircon petrochronology data set. See text for discussion and implications. The date in this figure are available in Table S7.

constrained geological setting with distinct endmember compositions. Despite these mitigating factors, the success of the NNT1 method remains tentative pending further confirmation with a larger data set. Nevertheless, this preliminary success lends confidence that use with larger data sets is also likely to be successful.

We conclude that the NNT1 method based on multiple measured variables from detrital zircon grains, along with the grain-source attribution based on maximum likelihood, are sound approaches to determining sedimentary provenance in complex settings. This conclusion opens up a number of potential applications and future directions. Most directly, this approach has applications to applied sedimentology with direct economic implications in exploring for Cu and potentially other ore bodies. We suggest that analysis of modern rivers or ancient sedimentary strata should enable identification of Cu-mobility indicators in the detrital zircon fraction. This can be traced upstream in modern rivers or mapped for ancient strata (Smith, Saylor, Lapen, Leary, & Sundell, 2023) to determine the locus of fluid-rich, oxidized intrusive bodies which may be Cu-fertile. However, the ability to correlate zircon geochemistry to specific lithologies (Belousova et al., 2002; Sundell et al., 2022) or to tectonic settings (Sundell et al., 2024) suggests that the multi-variate approach described herein will be a boon to provenance studies and tectonic reconstruction.

6. Conclusions

Application of non-negative Tucker-1 tensor decomposition (NNT1) opens the door to sediment source characterization and petrochronology of multivariate detrital zircon data sets. We demonstrate the ability of this novel method to yield geologically consistent and comprehensible results by tracking down-ice stream movement of zircons from ore-bearing (fertile) and non-ore-bearing (infertile) igneous rocks of the GCB in southern British Columbia. NNT1 of a multivariate geochemical data set from detrital zircons from till samples yields two endmembers whose geochemical distributions can be consistently understood in terms of derivation either non-

SAYLOR ET AL. 13 of 16

are governed by the applicable Creative Commons License

Acknowledgments

JES acknowledges "the Creator, the

perpetual order, the eternal and

fountain of all wisdom, the approver of

superessential spring of geometry and

harmonics," (Johannes Kepler, Harmonies

their editorial handling of this manuscript,

including recommendations that improved

the science. We also thank N.D. Perez and

two anonymous reviewers for detailed and

constructive reviews that helped to

strengthen the manuscript. The authors

thank L. Caracciolo, U. Schaltegger, and

two anonymous reviewers for comments

and reviews of an earlier version of this

manuscript. Funding for this research came

from Teck Resources Ltd., BHP Minerals

Canada Ltd., and the Natural Sciences and Engineering Research Council (NSERC)

through Alliance grant ALLRP

580390 - 22.

of the World) for the order identified by

this research. The authors thank Editor J. Sankey and Associate Editor H. Gray for oxidized and fluid-poor (i.e., low ore potential, Source 1) or oxidized and fluid-rich (i.e., potential ore bodies, Source 2) igneous rocks. Moreover, the proportions of the Source 2 endmember decrease with increasing distance from the ore bodies. Finally, we demonstrate that individual zircon grains can be ascribed to either Source 1 or 2 (i.e., low or high ore potential). Combining these results from an empirical data set with previously published results from an artificial data set suggests that the NNT1 method is a flexible, precise, and accurate method of characterizing unknown sediment sources. Finally, we present a free web-based application, DZgrainalyzer (http://dzgrainalyzer.eoas.ubc.ca/), built on the code described by Graham et al. (2025) and capable of conducting all of the analyses presented herein.

Conflict of Interest

The authors declare no conflicts of interest relevant to this study.

Data Availability Statement

All of the analyses presented herein can be freely accessed at http://dzgrainalyzer.eoas.ubc.ca/ or https://www.dzgrainalyzer.com. The source code is available at https://zenodo.org/records/17008872 or https://github.com/njericha/SedimentSourceAnalysis.jl/releases/tag/v1.1.1. Data are available from Saylor (2025): https://zenodo.org/records/16459710.

References

- Arnold, H., & Ferbey, T. (2020). Ice-flow indicator database, British Columbia and Yukon. *Volume British Columbia Geological Survey Open File 2020-03*, British Columbia Ministry of Energy and Mines and Petroleum Resources, 1.
- Arnold, H., Ferbey, T., & Hickin, A. S. (2016). Ice-flow indicator compilation, British Columbia and Yukon, British Columbia ministry of energy and mines, volume British Columbia geological survey open file 2016-04. *Geological Survey of Canada*, open file 8083, scale: 1:1,750,000.
- Ballard, J. R., Palin, M. J., & Campbell, I. H. (2002). Relative oxidation states of magmas inferred from Ce (IV)/Ce (III) in zircon: Application to porphyry copper deposits of northern Chile. *Contributions to Mineralogy and Petrology*, 144(3), 347–364. https://doi.org/10.1007/s00410-002-0402-5
- Belousova, E., Griffin, W., O'Reilly, S. Y., & Fisher, N. (2002). Igneous zircon: Trace element composition as an indicator of source rock type. Contributions to Mineralogy and Petrology, 143(5), 602–622. https://doi.org/10.1007/s00410-002-0364-7
- Bissig, T., Leal-Mejía, H., Stevens, R. B., & Hart, C. J. R. (2017). High Sr/Y magma petrogenesis and the link to porphyry mineralization as revealed by garnet-bearing I-Type granodiorite porphyries of the middle Cauca Au-Cu Belt, colombia *Economic Geology*, 112(3), 551–568. https://doi.org/10.2113/econgeo.112.3.551
- Bouzari, F., Hart, C., & Bissig, T. (2020). Assessing porphyry copper deposit fertility in British Columbia batholiths using zircons. In *Geoscience BC* report* (Vol. 8, pp. 1–24).
- Campbell, I. H., Reiners, P. W., Allen, C. M., Nicolescu, S., & Upadhyay, R. (2005). He-Pb double dating of detrital zircons from the ganges and indus Rivers: Implication for quantifying sediment recycling and provenance studies. *Earth and Planetary Science Letters*, 237(3–4), 402–432. https://doi.org/10.1016/j.epsl.2005.06.043
- Campbell, M. J., Rosenbaum, G., Allen, C. M., & Spandler, C. (2020). Continental crustal growth processes revealed by detrital zircon petro-chronology: Insights from Zealandia. *Journal of Geophysical Research: Solid Earth*, 125(8), e2019JB019075. https://doi.org/10.1029/2019jb019075
- Capaldi, T. N., Horton, B. K., McKenzie, N. R., Stockli, D. F., & Odlum, M. L. (2017). Sediment provenance in contractional orogens: The detrital zircon record from modern rivers in the Andean fold-thrust belt and foreland basin of Western Argentina. *Earth and Planetary Science Letters*, 479, 83–97. https://doi.org/10.1016/j.epsl.2017.09.001
- Carrasco-Godoy, C., Campbell, I. H., & Cajal, Y. (2024). Quantifying the criteria used to identify zircons from ore-bearing and barren systems in Porphyry copper exploration. *Economic Geology*, 119(5), 1035–1058. https://doi.org/10.5382/econgeo.5086
- Carroll, J. D., & Chang, J.-J. (1970). Analysis of individual differences in multidimensional scaling via an n-way generalization of "Eckart-Young" decomposition. *Psychometrika*, 35(3), 283–319. https://doi.org/10.1007/bf02310791
- Casselman, M., McMillan, W., & Newman, K. (1995). Highland Valley porphyry copper deposits near Kamloops, British Columbia: A review and update with emphasis on the Valley deposit: Canadian Institute of Mining. *Metallurgy and Petroleum*, 46, 161–191.
- Chapman, J. B., Ducea, M. N., DeCelles, P. G., & Profeta, L. (2015). Tracking changes in crustal thickness during orogenic evolution with Sr/Y: An example from the North American Cordillera. *Geology*, 43(10), 919–922. https://doi.org/10.1130/g36996.1
- Cherniak, D., Hanchar, J., & Watson, E. (1997a). Rare-earth diffusion in zircon. Chemical Geology, 134(4), 289–301. https://doi.org/10.1016/s0009-2541(96)00098-8
- Cherniak, D. J., Hanchar, J. M., & Watson, E. B. (1997b). Diffusion of tetravalent cations in zircon. Contributions to Mineralogy and Petrology, 127(4), 383–390. https://doi.org/10.1007/s004100050287
- Clague, J. J., & Ward, B. (2011). Chapter 44 Pleistocene glaciation of British Columbia. In J. Ehlers, P. L. Gibbard, & P. D. Hughes (Eds.), Developments in Quaternary sciences (Vol. 15, pp. 563–573). Elsevier. https://doi.org/10.1016/b978-0-444-53447-7.00044-1
- Clark, P. U. (1987). Subglacial sediment dispersal and till composition. *The Journal of Geology*, 95(4), 527–541. https://doi.org/10.1086/629147 D'Angelo, M., Miguel, A., Hollings, P., Byrne, K., Piercey, S., & Creaser, R. A. (2017). Petrogenesis and magmatic evolution of the Guichon Creek batholith: Highland Valley porphyry Cu±(Mo) district, south-central British Columbia. *Economic Geology*, 112(8), 1857–1888. https://doi.org/10.5382/econgeo.2017.4532
- Davidson, J., Turner, S., Handley, H., Macpherson, C., & Dosseto, A. (2007). Amphibole "sponge" in arc crust? *Geology*, 35(9), 787–790. https://doi.org/10.1130/g23637a.1

SAYLOR ET AL. 14 of 16

- Dickinson, W. R., Lawton, T. F., & Gehrels, G. E. (2009). Recycling detrital zircons: A case study from the Cretaceous Bisbee Group of southern Arizona: Geology. *Geology*, 37(6), 503–506. https://doi.org/10.1130/g25646a.1
- Dilles, J. H., Kent, A. J., Wooden, J. L., Tosdal, R. M., Koleszar, A., Lee, R. G., & Farmer, L. P. (2015). Zircon compositional evidence for sulfur-degassing from ore-forming arc magmas. *Economic Geology*, 110(1), 241–251. https://doi.org/10.2113/econgeo.110.1.241
- Ferbey, T., & Arnold, H. (2013). Compilation of Micro-to macro-scale ice-flow indicators for the interior Plateau. Central British Columbia.
 Ferbey, T., Plouffe, A., & Bustard, A. L. (2016). Geochemical, mineralogical, and textural data from tills in the Highland Valley Copper mine area, south-central British Columbia (Vol. 11). British Columbia Geological Survey GeoFile.15.
- Gehrels, G., & Pecha, M. (2014). Detrital zircon U-Pb geochronology and Hf isotope geochemistry of Paleozoic and Triassic passive margin strata of western North America. Geosphere, 10(1), 49–65.
- Gower, J. C. (1975). Generalized procrustes analysis. Psychometrika, 40(1), 33-51. https://doi.org/10.1007/bf02291478
- Graham, N., Richardson, N., Friedlander, M. P., & Saylor, J. E. (2025). Tracing sedimentary origins in multivariate geochronology via constrained tensor factorization. *Mathematical Geosciences*, 57(4), 601–628. https://doi.org/10.1007/s11004-024-10175-0
- Hoskin, P. W. O., & Schaltegger, U. (2003). The composition of Zircon and igneous and metamorphic petrogenesis. Reviews in Mineralogy and Geochemistry, 53(1), 27–62. https://doi.org/10.2113/0530027
- Iverson, N. R., Hooyer, T. S., & Hooke, R. L. (1996). A laboratory study of sediment deformation: Stress heterogeneity and grain-size evolution. Annals of Glaciology, 22, 167–175. https://doi.org/10.3189/1996aog22-1-167-175
- Jackson, L. J., & Horton, B. K. (2025). Sediment provenance signatures of the largest river in the Andes (Marañón River, Peru): Implications for signal propagation in the Amazon drainage system. *Journal of South American Earth Sciences*, 157, 105471. https://doi.org/10.1016/j.jsames. 2025.105471
- Kohn, M. J., Engi, M., & Lanari, P. (2017). Petrochronology: Methods and applications. Mineralogical Society of America Reviews in Mineralogy and Geochemistry, 83(1), 575. https://doi.org/10.2138/rmg.2017.83.0
- Lee, C.-T. A., & Tang, M. (2020). How to make porphyry copper deposits. Earth and Planetary Science Letters, 529, 115868. https://doi.org/10.1016/j.epsl.2019.115868
- Lee, R. G., Byrne, K., D'Angelo, M., Hart, C. J., Hollings, P., Gleeson, S. A., & Alfaro, M. (2021). Using zircon trace element composition to assess porphyry copper potential of the Guichon Creek batholith and Highland Valley Copper deposit, south-central British Columbia. Mineralium Deposita, 56(2), 215–238. https://doi.org/10.1007/s00126-020-00961-1
- Lee, R. G., Dilles, J. H., Tosdal, R. M., Wooden, J. L., & Mazdab, F. K. (2017). Magmatic evolution of granodiorite intrusions at the El Salvador porphyry copper deposit, Chile, based on trace element composition and U/Pb age of zircons. *Economic Geology*, 112(2), 245–273. https://doi.org/10.2113/econgeo.112.2.245
- Lee, R. G., Plouffe, A., Ferbey, T., Hart, C. J., Hollings, P., & Gleeson, S. A. (2021b). Recognizing porphyry copper potential from till zircon composition. In A case study from the Highland Valley Porphyry District, south-central British Columbia. Economic Geology.
- Loader, M. A., Nathwani, C. L., Wilkinson, J. J., & Armstrong, R. N. (2022). Controls on the magnitude of Ce anomalies in zircon. Geochimica et Cosmochimica Acta, 328, 242–257. https://doi.org/10.1016/j.gca.2022.03.024
- Loucks, R. (2014). Distinctive composition of copper-ore-forming arcmagmas. Australian Journal of Earth Sciences, 61(1), 5–16. https://doi.org/10.1080/08120099.2013.865676
- Loucks, R. R., Fiorentini, M. L., & Henríquez, G. J. (2020). New magmatic oxybarometer using trace elements in Zircon. *Journal of Petrology*, 61(3), egaa034. https://doi.org/10.1093/petrology/egaa034
- Loucks, R. R., Henríquez, G. J., & Fiorentini, M. L. (2024). Zircon and whole-rock trace element indicators of magmatic hydration state and oxidation state discriminate copper ore-forming from Barren Arc Magmas. *Economic Geology*, 119(3), 511–523. https://doi.org/10.5382/econgeo.5071
- Lu, Y., Loucks, R., Fiorentini, M., McCuaig, T., Evans, N. J., Yang, Z.-M., et al. (2016). Zircon compositions as a pathfinder for porphyry Cu±Mo±Au deposits (Vol. 19, pp. 329–347). Society of Economic Geologists. Special Publications Series.
- Matmon, A., Haeussler, P. J., & Team, A. (2020). Sediment sources and transport by the Kahiltna Glacier and other catchments along the south side of the Alaska Range, Alaska. *Geosphere*, 16(3), 787–805. https://doi.org/10.1130/ges02190.1
- McMillan, W., Anderson, R., Chan, R., & Chow, W. (2009). Geology and mineral occurrences (minfile). In *Guichon Creek batholith and Highland Valley porphyry copper district*. Open File, v. 6079.
- Moore, G., & Carmichael, I. S. E. (1998). The hydrous phase equilibria (to 3 kbar) of an andesite and basaltic andesite from Western Mexico: Constraints on water content and conditions of phenocryst growth. *Contributions to Mineralogy and Petrology*, 130(3), 304–319. https://doi.org/10.1007/s004100050367
- Pizarro, H., Campos, E., Bouzari, F., Rousse, S., Bissig, T., Gregoire, M., & Riquelme, R. (2020). Porphyry indicator zircons (PIZs): Application to exploration of porphyry copper deposits. *Ore Geology Reviews*, 126, 103771. https://doi.org/10.1016/j.oregeorev.2020.103771
- Plouffe, A., Ferbey, T., Hashmi, S., & Ward, B. C. (2016). Till geochemistry and mineralogy: Vectoring towards Cu porphyry deposits in British Columbia, Canada. Geochemistry: Exploration, Environment, Analysis, 16(3-4), 213-232. https://doi.org/10.1144/geochem2015-398
- Plouffe, A., McClenaghan, M. B., Paulen, R. C., McMartin, I., Campbell, J. E., & Spirito, W. A. (2013). Processing of glacial sediments for the recovery of indicator minerals: Protocols used at the geological survey of Canada. *Geochemistry: Exploration, Environment, Analysis*, 13(4), 303–316. https://doi.org/10.1144/geochem2011-109
- Rubatto, D. (2002). Zircon trace element geochemistry: Partitioning with garnet and the link between U–Pb ages and metamorphism. *Chemical Geology*, 184(1–2), 123–138. https://doi.org/10.1016/s0009-2541(01)00355-2
- Saylor, J. E. (2025). Tracking Cu-fertile sediment sources via multivariate petrochronological mixture modelling of detrital zircons [Dataset]. https://doi.org/10.5281/zenodo.16459710
- Saylor, J. E., Knowles, J. N., Horton, B. K., Nie, J. S., & Mora, A. (2013). Mixing of source populations recorded in detrital zircon U-Pb age Spectra of modern river sands. The Journal of Geology, 121(1), 17–33. https://doi.org/10.1086/668683
- Saylor, J. E., & Sundell, K. E. (2016). Quantifying comparison of large detrital geochronology data sets. *Geosphere*, 12(1), 203–220. https://doi.org/10.1130/ges01237.1
- Saylor, J. E., & Sundell, K. E. (2021). Tracking Proterozoic-Triassic sediment routing to western Laurentia via bivariate non-negative matrix factorization of detrital provenance data. Journal of the Geological Society.
- Saylor, J. E., Sundell, K. E., & Sharman, G. R. (2019). Characterizing sediment sources by non-negative matrix factorization of detrital geochronological data. Earth and Planetary Science Letters, 512, 46–58. https://doi.org/10.1016/j.epsl.2019.01.044
- Schaetzl, R. J., Baish, C., Colgan, P. M., Knauff, J., Bilintoh, T., Wanyama, D., et al. (2020). A sediment-mixing process model of till genesis, using texture and clay mineralogy data from Saginaw lobe (Michigan, USA) tills. *Quaternary Research*, 94, 174–194. https://doi.org/10.1017/gua.2019.82

SAYLOR ET AL. 15 of 16

- Schaltegger, U., & Davies, J. H. F. L. (2017). Petrochronology of Zircon and Baddeleyite in igneous rocks: Reconstructing magmatic processes at high temporal resolution. *Reviews in Mineralogy and Geochemistry*, 83(1), 297–328. https://doi.org/10.2138/rmg.2017.83.10
- Sisson, T. (1994). Hornblende-melt trace-element partitioning measured by ion microprobe. Chemical Geology, 117(1–4), 331–344. https://doi.org/10.1016/0009-2541(94)90135-x
- Smith, T. M., Saylor, J. E., Lapen, T. J., Hatfield, K., & Sundell, K. E. (2023). Identifying sources of non-unique detrital age distributions through integrated provenance analysis: An example from the Paleozoic central Colorado trough. *Geosphere*, 19(2), 471–492. https://doi.org/10.1130/ges02541.1
- Smith, T. M., Saylor, J. E., Lapen, T. J., Leary, R. J., & Sundell, K. E. (2023). Large detrital zircon data set investigation and provenance mapping: Local versus regional and Continental sediment sources before, during, and after Ancestral Rocky Mountain deformation. GSA Bulletin. https://doi.org/10.1130/b36285.1
- Sundell, K., Saylor, J. E., & Pecha, M. (2019). Provenance and recycling of detrital zircons from Cenozoic Altiplano strata and the crustal evolution of western South America from combined U-Pb and Lu-Hf isotopic analysis. In B. K. Horton & A. Folguera (Eds.), *Andean tectonics* (pp. 363–397). Flsevier
- Sundell, K. E., George, S. W. M., Carrapa, B., Gehrels, G. E., Ducea, M. N., Saylor, J. E., & Pepper, M. (2022). Crustal thickening of the Northern central Andean Plateau inferred from trace elements in Zircon. *Geophysical Research Letters*, 49(3), e2021GL096443. https://doi.org/10.1029/2021gl096443
- Sundell, K. E., Macdonald, F. A., & Puetz, S. J. (2024). Does zircon geochemistry record global sediment subduction? (Vol. 52, pp. 282–286) Geology. https://doi.org/10.1130/g51817.1
- Sundell, K. E., & Saylor, J. E. (2017). Unmixing detrital geochronology age distributions: Geophysics. Geochemistry, Geosystems, 18(8), 2872–2886. https://doi.org/10.1002/2016gc006774
- Tang, M., Ji, W.-Q., Chu, X., Wu, A., & Chen, C. (2020). Reconstructing crustal thickness evolution from europium anomalies in detrital zircons. *Geology*, 49(1), 76–80. https://doi.org/10.1130/g47745.1
- Vermesch, P., & Garzanti, E. (2015). Making geological sense of "Big Data" in sedimentary provenance analysis. Chemical Geology, 409, 20–27. https://doi.org/10.1016/j.chemgeo.2015.05.004
- Vermeesch, P., Lipp, A. G., Hatzenbühler, D., Caracciolo, L., & Chew, D. (2023). Multidimensional scaling of varietal data in sedimentary provenance analysis. *Journal of Geophysical Research: Earth Surface*, 128(3), e2022JF006992. https://doi.org/10.1029/2022jf006992
- Watson, E., Wark, D., & Thomas, J. (2006). Crystallization thermometers for zircon and rutile. *Contributions to Mineralogy and Petrology*, 151(4), 413–433. https://doi.org/10.1007/s00410-006-0068-5

SAYLOR ET AL. 16 of 16